Monitoring deformation from hydrologic processes in a karst aquifer using long-baseline tiltmeters

Thomas Jacob, Jean Chery, Frederick Boudin, Roger Bayer

Monitoring deformation from hydrologic processes in a karst aquifer using long-baseline tiltmeters

Thomas Jacob,[1,2] Jean Chéry,[1] Frédéric Boudin,[1] and Roger Bayer[1]

Received 6 April 2009; revised 18 March 2010; accepted 13 May 2010; published 30 September 2010.

[1] The aim of this study is to bring new information on water storage dynamics in karst systems from tiltmeter measurements. Newly developed long-base hydrostatic tiltmeters are installed at two sites on the Larzac plateau (France) in a karst aquifer of ~100 km^2 recharge area. Each site is located within a karst cave where two tilt directions are monitored. Significant reversible tilt deformation reaching amplitudes of 10^{-6} to 10^{-5} rad was observed at both sites following heavy precipitation. Elastic parameters were determined with an experiment in which a tiltmeter site was loaded by up to 25 t of weight at strategic locations at the ground surface. Mechanisms responsible for the observed tilt were then examined by means of finite element modeling. Deformation induced by water pressure changes in fractures is our preferred interpretation as the most plausible mechanism. Within this scope, we used the tiltmeter responses to extract time constants using lumped parameter modeling. Time constants are interpreted to be associated with the filling and emptying of fractures nearby the tiltmeters. These instruments therefore appear as useful tools to study the local dynamics of water infiltration in karst systems.

Citation: Jacob, T., J. Chéry, F. Boudin, and R. Bayer (2010), Monitoring deformation from hydrologic processes in a karst aquifer using long-baseline tiltmeters, *Water Resour. Res.*, *46*, W09542, doi:10.1029/2009WR008082.

1. Introduction

[2] Because of their structural heterogeneity, karst systems are complex hydrological systems whose spring hydrographs are classically analyzed and modeled to obtain information. Such systems are conceptually divided into three horizons: epikarst, infiltration zone, and saturated or phreatic zones [*Mangin*, 1975]. The spring discharge is characterized by two regimes: high flow following precipitation and base flow during drier periods. High flow events are due to fast water infiltration to the phreatic zone through enlarged drainage shafts and are short-lived (typically 5 to 20 days). Base flow discharge is sustained by groundwater storage within the karst and may last several months. Two main approaches are adopted to simulate karst spring hydrographs: physical modeling and lumped parameter modeling. Physical modeling using water transfer equations requires a detailed knowledge of the internal geometry and physical properties of the system, which is rarely the case [*Jeannin*, 2001]. Lumped parameter modeling is based on (1) black or gray box models using deconvolution or a transfer function between rainfall and spring discharge [*Denic-Jukic and Jukic*, 2003; *Jukic and Denic-Jukic*, 2006; *Labat et al.*, 2000a, 2000b] or (2) lumped reservoir models where discharge equations link water levels between lumped reservoirs on the basis of conceptual models [*Fleury et al.*, 2007a, 2007b]. These models bring information on the overall behavior of karst systems and reveal the existence of reservoirs with different discharge time constants. Local water transfer may not be obtained with these models using basin scale fluxes such as rainfall or spring discharge.

[3] Water transfer within karst systems involves flow between pores, fractures of variable apertures, and large conduits. This can lead to highly variable saturation, and data such as borehole water levels are often difficult to interpret. Geophysical methods such as electrical resistivity and magnetic resonance soundings [*Legchenko et al.*, 2002] bring local information on water storage but are rarely implemented as continuous monitoring tools. Furthermore, such methods have limited resolution and investigation depths. Recently, gravity variations have been used to quantitatively estimate the water storage variations in a karst system [*Jacob et al.*, 2008, 2009; *Van Camp et al.*, 2006]. However, both the lack of continuous acquisition and the nonuniqueness of gravity interpretation relative to depth make interpretations uncertain in terms of water transfer.

[4] A way to infer water transfer in a permeable medium is to study its impact on the deformation of the solid medium using high resolution tiltmeters [*Fabian and Kümpel*, 2003]. Long-base tiltmeters measure the difference in vertical displacement with respect to a gravity equipotential surface over a baseline typically 5 to 200 m in length. Since the pioneering work of *Michelson* [1914], interferometric instrument development has progressed to show a stability better than 10^{-8} rad/month with low noise levels (better than 10^{-10} rad) [*Boudin et al.*, 2008; *d'Oreye and Zurn*, 2005]. Tilt deformation of a hydrological nature has been considered noise for geophysicists [*Dal Moro and Zadro*, 1998; *Yamauchi*, 1987; *Zadro and Braitenberg*, 1999]. However, tiltmeters have recently been set up for

[1]Géosciences Montpellier, UMR CNRS/UM2 5243, Université Montpellier II, Montpellier, France.
[2]Also at Department of Physics and Cooperative Institute for Research in Environmental Sciences, University of Colorado, Boulder, Colorado, USA.

0043-1397/10/2009WR008082

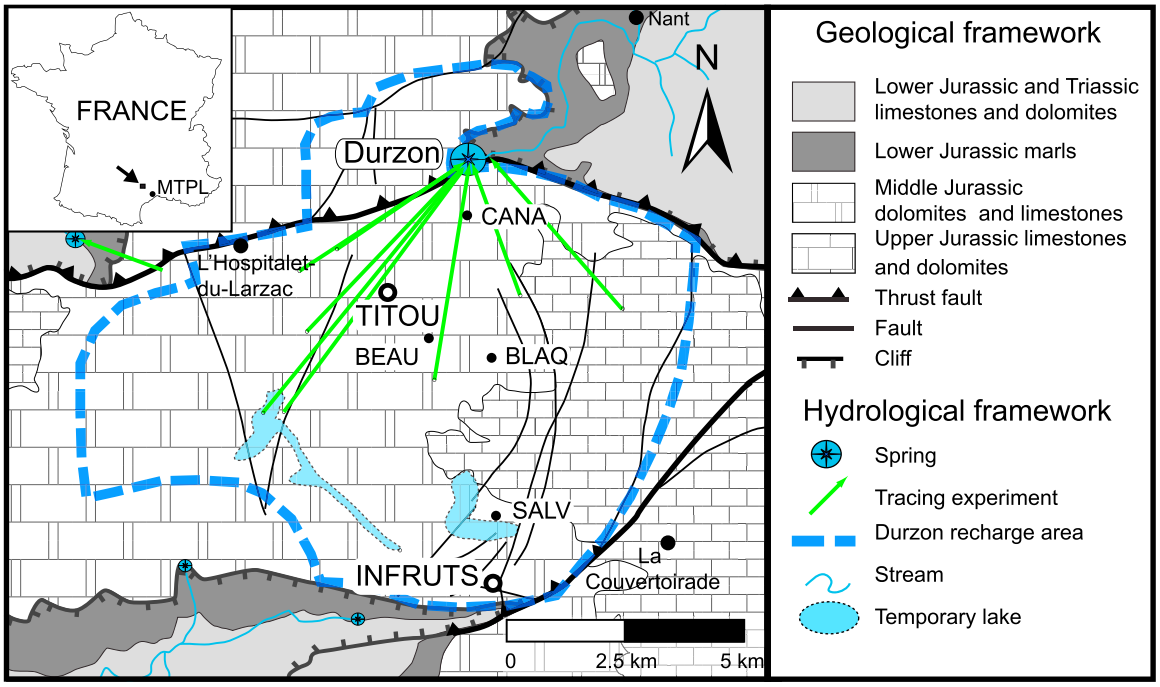

Figure 1. Hydrogeological setting of the karst system; tiltmeter location is given by open circles. SALV, BLAQ, BEAU, and CANA correspond to absolute gravity measurement sites.

the specific study of hydrology. Deformation due to pore pressure changes has been monitored with this technique [*Fabian and Kümpel*, 2003; *Weise et al.*, 1999; *Westerhaus and Welle*, 2002]. Water also acts as a load that deforms the upper crust, and such loading has been inferred to cause deformation measured by tiltmeters at the hydrological basin scale [*Longuevergne*, 2008]. Also, water level variation in a hydraulically active fracture close to a tiltmeter was identified as a distinct source of deformation [*Evans and Wyatt*, 1984; *Longuevergne et al.*, 2009].

[5] In this study, data from two sets of long-base hydrostatic tiltmeters installed in caves within a karst system are analyzed. The instruments exhibit tilt responses associated with rainfall. We explore the possible physical mechanisms responsible for this signal. We first determine elastic constants at one site with a loading experiment. Using a finite element elastic model, tilts generated from both surface loading and deformation induced from water pressure changes in fractures are then compared to observed tilt amplitudes. Finally, observed time responses are accounted for using lumped parameter modeling comprising soil and fracture reservoirs.

2. Site Description and Instrumentation

2.1. The Durzon Karst System

[6] The Durzon karst system is located in the Grands Causses area, southern French Massif Central. This aquifer is embedded in a 400 m thick formation of middle to upper Jurassic limestones and dolomites deposited on top of a 200 m thick upper Liassic marl formation [*Bruxelles*, 2001b] (Figure 1). This latter formation acts as a low-permeability barrier, which defines the lower limit of the saturated zone of the karst system. Middle Jurassic formations are exposed in the recharge area, particularly a 200 m thick dolomite formation of Bathonian age, which largely outcrops.

[7] Recharge water for the Durzon karst system exclusively comes from rainfall, which infiltrates at the surface of the plateau with a catchment surface of ~100 km^2 at a mean elevation of 750 m. Discharge occurs at the Durzon Spring at 533 m elevation. Thanks to monitoring by the Parc Naturel Régional des Grands Causses, this perennial spring is known to have a mean daily discharge of 1.4 m^3 s^{-1} (calculated over the 2002–2007 period) with maximum daily discharges reaching 18 m^3 s^{-1} during high-flow events. According to a well-accepted conceptual model [*Mangin*, 1975], a karst system may be horizontally layered into three zones: (1) The epikarst zone, including both soil and weathered rock, has 5–30 m depth; this zone has a high secondary porosity and is expected to be an important water reservoir [*Williams*, 1983, 2008]; (2) the infiltration zone below is mostly composed of massive rock with penetrative fissures and conduits, therefore making fast vertical water transfer possible; and (3) the saturated or phreatic zone formed by large conduits ensures a mostly horizontal water flow to the outlet.

[8] The three aforementioned zones may show important water storage changes, depending on the studied karst [*Bakalowicz*, 2005]. On the Durzon karst system, surface to depth microgravity measurements coupled to surface absolute gravity measurements have provided insights on epikarst water storage changes occurring in the BLAQ area (see Figure 1) [*Jacob et al.*, 2008, 2009].

[9] The Durzon spring hydrograph is characterized by high-flow events following important precipitation as well as a base flow component. High-flow events necessitate fast water infiltration to the phreatic zone through drainage shafts and are typically short-lived. Base flow discharge varies seasonally and is sustained by diffuse groundwater

Table 1. Tiltmeter Specifications for the Sites TITOU and INFRUTS

Site	Depth (m)	Latitude	Longitude	Azimuth (°)	Length (m)	Code Name
TITOU	50	43.96245	3.24095	12	10.8	T012
				94	24.9	T094
INFRUTS	16	43.90484	3.26679	111	8.9	I111
				144	4.7	I144

storage within the secondary porosity, fissures, or large open voids in the karst.

[10] During exceptionally long rainfall periods, temporary lakes (shown in blue in Figure 1) appear at the south of the recharge area [*Bruxelles*, 2001b; *Plagnes*, 1997], their last appearance being in 1996. These lakes form when precipitation exceeds the infiltration capacity of the epikarst and infiltration zone toward the saturated zone [*Bruxelles*, 2001b; *Plagnes*, 1997; *Ricard and Bakalowicz*, 1996]. The vadose zone, including the epikarst and infiltration zone, has therefore a different behavior in the north and south of the recharge area. It is well drained in the north and poorly drained in the south (Figure 1) [*Bruxelles*, 2001a; *Ricard and Bakalowicz*, 1996].

2.2. Instruments and Site Description

[11] Long-base hydrostatic tiltmeters have been installed at two sites called TITOU and INFRUTS on the Durzon karst system (Figure 1). A hydrostatic tiltmeter consists of a tube connecting two vessels filled with water (for a review, see *Agnew* [1986] and *Zadro and Braitenberg* [1999]). The differential change in water level in the two vessels is monitored to calculate tilt. These water level changes are caused by differential vertical displacement of the rock mass between the two vessels and, to a lesser extent, by the tilting of the gravity equipotential surface that coincides with the water surface in the vessels. Therefore tiltmeters are relative instruments that measure strain relative to an initial state. To evaluate tilt as precisely as possible, special attention is given to the coupling between the instrument and the surrounding rock. Niches were dug in the rock faces so that the tiltmeter vessels were in direct contact with the rock. Such instruments are already installed in horizontal mine tunnels and display a short-term resolution of 10^{-9} rad and a stability of 10^{-8} rad/month under appropriate thermal regimes [*Longuevergne et al.*, 2009]. The technical description of these instruments can be found elsewhere [*Boudin*, 2004; *Boudin et al.*, 2008].

[12] Two sets of tiltmeters were installed within each site. The TITOU site is located at the north of the recharge area (Figure 1), where two tiltmeters were installed in July 2006 at 50 m depth with an orientation of N012° (T012) and N094° (T094) and lengths of 10.8 and 24.9 m, respectively (Table 1 and Figure 2). The INFRUTS site is located close to the southern boundary of the recharge area. Its two tiltmeters are oriented at N111° (I111) and N144° (I144) with lengths of 8.9 and 4.7 m, respectively (Table 1 and Figure 2). This latter site was set up in June 2007 at 16 m depth.

[13] It should be emphasized that the two sites are in different configurations: (1) The depth of the TITOU site (50 m) is 3 times greater than that of the INFRUTS site (16 m; see Table 1). (2) The length of the TITOU T094 tiltmeter is nearly 25 m, whereas the longest instrument at INFRUTS (I111) is 8.9 m in length. (3) The TITOU site area is characterized by a well-drained infiltration zone, with potholes and cave systems reaching the phreatic zone located some 150 to 180 m below the ground surface. By contrast, the INFRUTS site is located in a poorly drained region where the impervious marls are relatively shallow (~100 m) compared with the rest of the recharge area [*Bruxelles*, 2001b]. Temporary lakes near INFRUTS are testimony to the poor drainage (see Figure 1). Also, systems of conduits and shafts are poorly developed at the INFRUTS area.

3. Tilt Data

3.1. Tilt Processing and Analysis

[14] Tilt data were recorded with a 2 min sampling rate. Data were first corrected for steps, then Earth tides and

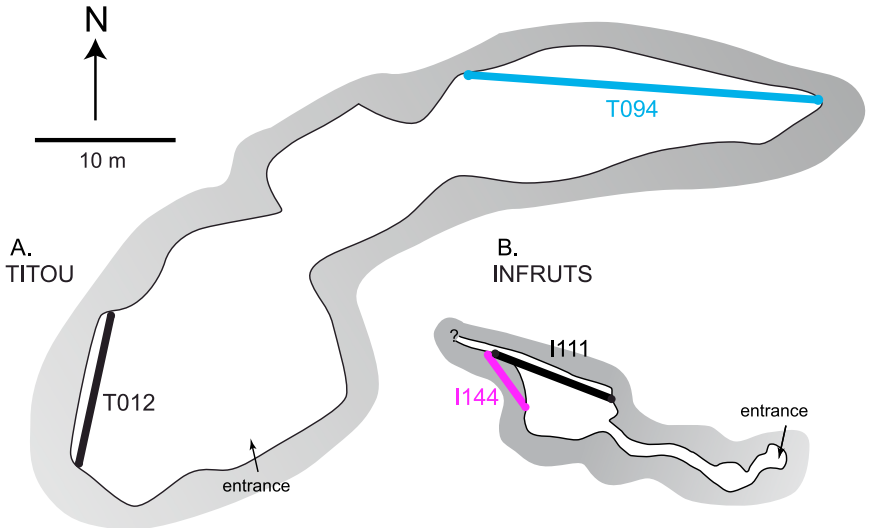

Figure 2. Map view of tiltmeter sites. Straight lines represent tiltmeter location on the rock face. Thin lines contoured in gray represent the two cave chambers that can be reached from the surface through potholes. The same scale is used for the two sites.

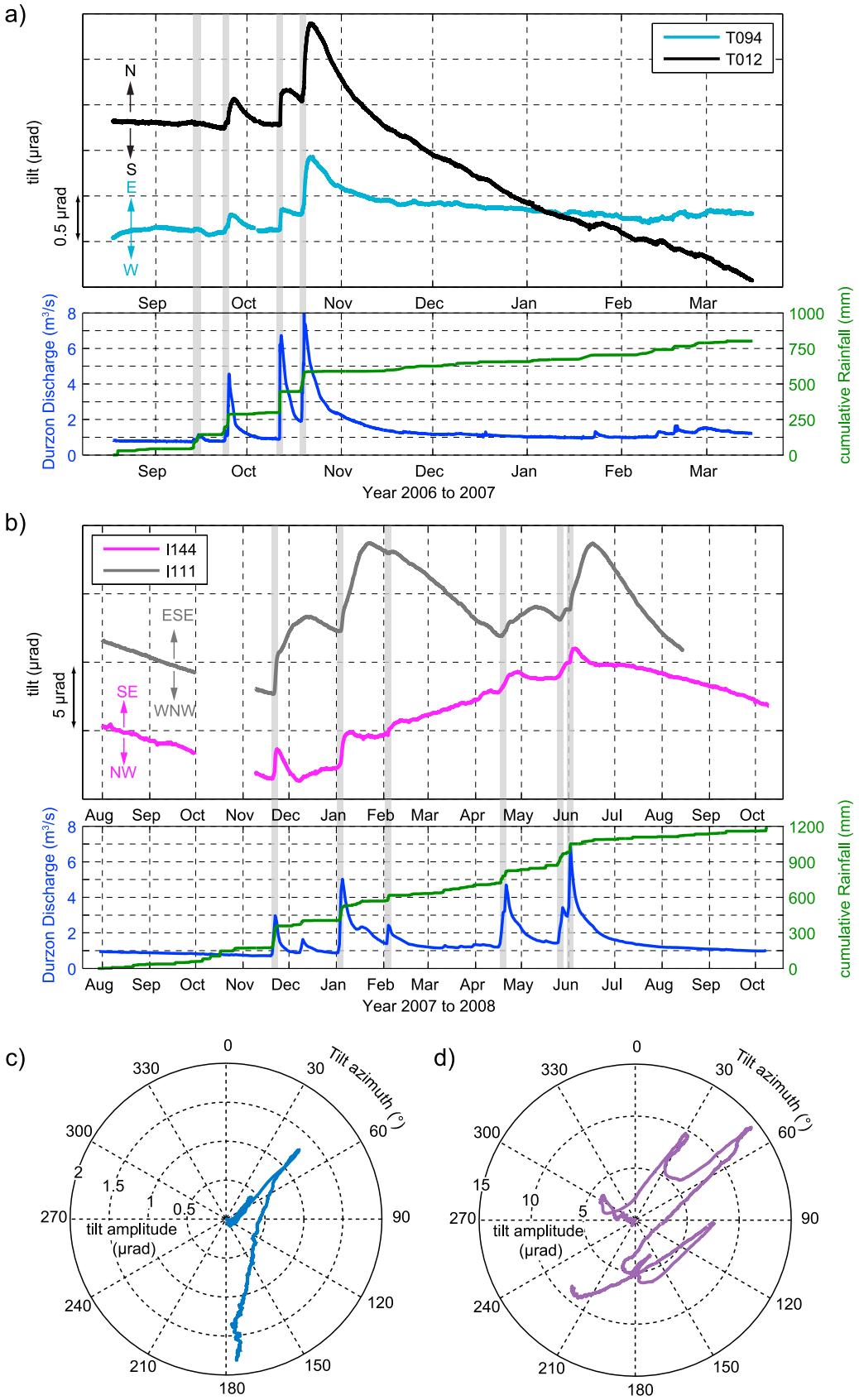

Figure 3. (a) Tilt time series from TITOU sites and (b) INFRUTS sites compared to cumulative rainfall and Durzon spring discharge. Gray-shaded lines mark important precipitation events. The same tilt series are represented in a stereo plot showing tilt amplitude versus azimuth for (c) TITOU tiltmeters and (d) INFRUTS tiltmeters.

Table 2. Mean Time Lags Between Maximum Tilt for All Tiltmeters and Both Rainfall and Maximum Durzon Discharge[a]

	Lag Versus Rainfall (d)	Lag Versus Discharge (d)
T012	2.6	1.7
T094	1.9	1.1
I111	20.1	17.9
I144	4.2	2.0

[a]Used events represented in Figures 3a and 3b as gray shaded area.

ocean loading effects were analyzed and corrected using ETERNA software [*Wenzel*, 1996]. The data were then aggregated to hourly averages giving the time series in Figure 3. For each instrument, the first month of acquisition was systematically discarded as it corresponds to the hydromechanical relaxation of the instrument that has neither geophysical nor hydrological significance. Gaps in all four tiltmeters' time series shown in Figure 3 are due to power failures. During the 23 month measurement period at the TITOU site, some other data were not used because of technical difficulties that made the recordings unreliable. For tiltmeter T012, a drift starting in November 2006 and still ongoing today is observed, with an average value of –0.48 μrad/month. Although we are not certain of the causes for this drift, instrumental or natural, we consider any external hydrological signal following its onset to be uncertain. The data recorded after mid-November 2006 are therefore disregarded in our analysis. For T094, we consider the data reliable until April 2007, when a sensor malfunctioned, hence making the signal unreliable. Tilt from long-base hydrostatic tiltmeter scales with the differential water level changes was measured in the two vessels; sensor malfunction in any of the vessels therefore renders the tilt measurement uncertain. At INFRUTS, tiltmeter I111 had one of its sensors malfunction starting in mid-August 2008, and data thereafter were discarded.

[15] Within the reliable data set, significant tilt signal is observed associated with significant precipitation events (Figure 3). Several events with common features can be identified on all four tiltmeters after large rainfall events. The tilts form asymmetrical pulses with steep rising limbs followed by slower decreasing ones. As has been observed for other rainfall-induced signals [*Braitenberg*, 1999], amplitude and phase associated with this signal are different for each site. The maximum tilt for each pulse response seems in phase for the TITOU tiltmeters, whereas the INFRUTS tiltmeters are distinctively out of phase, with each instrument reaching maximum tilt values at different times. Furthermore, signal amplitudes are different for each site, with tilts reaching some 10 μrad in amplitude at INFRUTS but only 1 μrad at TITOU. The tilt data are now compared with hydrological data to evaluate correlation to rainfall and spring discharge.

3.2. Comparison With Hydrological Data

[16] Tilt time series for both sites are now analyzed with respect to Durzon spring discharge and rainfall data (Figure 3). Spring discharge is monitored by the Parc National des Grands Causses (PNGC), and rainfall data are measured at BLAQ station with quarter-hourly time steps (Figure 1). Changes in tilt are associated with precipitation (Figures 3a and 3b; gray-shaded lines mark precipitation), but there is no simple linear relationship between rainfall and tilt amplitude. This is well illustrated by comparing mid-September 2006 rainfall events (~150 mm), which caused tilt amplitude <0.1 μrad at TITOU, with rainfall of similar magnitude later in September, which caused tilts of 0.2–0.8 μrad (Figure 3a). A similar behavior is observed in the spring discharge, which is greater after the second rain event than the first one. Spring discharge and tilt both appear to be dependent on antecedent conditions whereby they depend on both past and present hydrological events.

[17] The asymmetrical pulse response seems to be triggered by rainfall. As can shown in Figures 3a and 3b, the maximum tilts for each pulse response lag behind peaks of rainfall and spring discharge. The average lags for all identified events are given in Table 2. TITOU tiltmeters reach maximum tilts 2.6 and 1.9 days after rainfall and lag Durzon discharge maxima by 1.7 and 1.1 days for T012 and T094, respectively. INFRUTS tiltmeters reach maximum tilts 20.1 and 4.2 days after rainfall and lag Durzon discharge maxima by 18.0 and 2.0 days for I111 and I144, respectively.

[18] The maximum pulse responses for the TITOU tiltmeters occur almost simultaneously, but those of INFRUTS instruments are separated by more than 2 weeks, reaching maxima 20 days and 4.2 days after rainfall. Comparison to Durzon spring discharge is also informative. Pulse tilt signals and spring high flow events occur after the same precipitation events (Figure 3) yet with different temporal behavior (Table 2).

[19] Installing two long-base tiltmeters per site allows monitoring tilt in two directions defined by the baselines, defining two tilt vectors. The normal vector to these tilt vectors characterizes a plane whose tilt amplitude and azimuth represent the maximum tilt amplitude and its direction in space. We arbitrarily define the initial condition of these planes as horizontal. Maximum tilt amplitude as a function of tilt azimuth is represented in a stereo plot for TITOU and INFRUTS tiltmeters in Figures 3c and 3d. Because T094 and T012 react almost in phase and have similar tilt pulse responses for each major rainfall event, tilt azimuth remains constant in the N045° direction, reaching an amplitude of 1.3 μrad at the peak of the third tilt event (Figure 3c). The drift in T012 data is clearly seen in the southward trending tilt azimuth in Figure 3c. Tilt magnitude and direction at INFRUTS follows a more complicated pattern: The tiltmeters are out of phase and show different behavior. However, the pole of the tilt plane rises and falls in the N040° to N050° direction (Figure 3d) after major rainfall events. These events correspond to I111 asymmetrical pulse signals; four events are clearly identifiable on Figure 3d. Hydrology-induced tilt deformation has been identified as having fixed directions for various settings [*Braitenberg et al.*, 2006; *Yamauchi*, 1987], and our measurements compare favorably to these observations.

[20] We acknowledge the existence of atmospheric pressure-induced tilt deformation, yet its amplitude is generally 1 order of magnitude lower than that of hydraulically induced tilt [*Dal Moro and Zadro*, 1998]. Atmospheric pressure-induced tilt may have an amplitude of some 10^{-8} rad [*Boudin*, 2004; *Longuevergne*, 2008]. It is therefore safe to assert that the observed tilt signal is chiefly hydraulically induced.

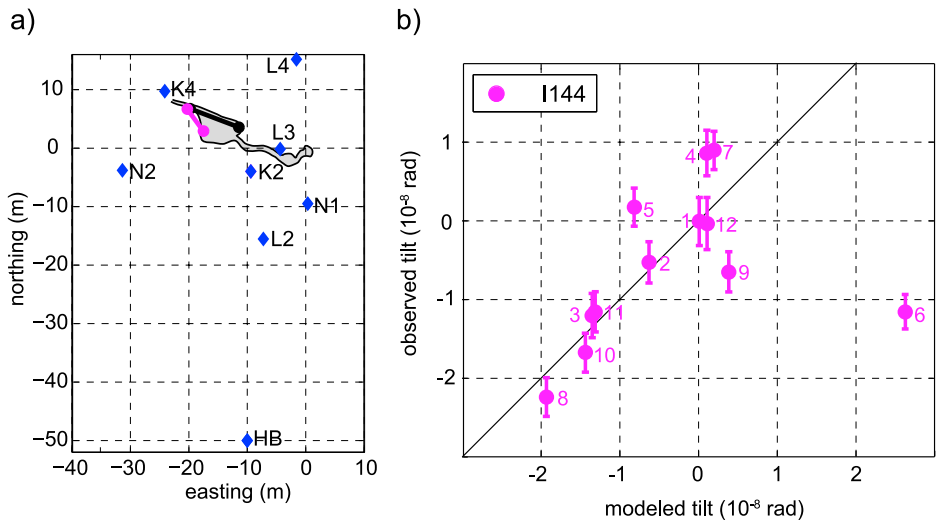

Figure 4. (a) Location map of INFRUTS loading experiment with the loading sites represented as blue diamonds. Tiltmeters and the cave are represented. (b) Observed tilt versus modeled tilt for best fitting elastic parameters for I144 tiltmeter. Error bars represent the standard deviation of the signal during each site loading. Numbers represent the load chronology in Table 3.

3.3. Tilt Time Responses

[21] The tilt signal is made up of different time responses. The asymmetrical pulse responses do not account entirely for the observed tilt signal. The signal of the TITOU site can be decomposed into two distinct time responses (see Figure 3a):

[22] 1. A short-term response expressed by pulses, with three clearly identified events, and maximum amplitudes reaching ~1 μrad, and

[23] 2. A longer-term time response that starts after the mid-October 2006 rainfalls and is characterized by a decrease from November 2006 to March 2007 in T094. Peak amplitude of this signal is <0.5 μrad. Because of the overlapping of these two signals, the long-term trend shape is ambiguous. T012 can be decomposed in the same manner as T094, but the decrease after November 2006 is important, reaching some 2 μrad.

[24] For INFRUTS tiltmeters, a similar decomposition can be done. I144 signal can be decomposed into short and long-term signals. The short-term signal is a series of pulses, and the long-term signal shows a minimum in December 2007 and a maximum in July 2008 (Figure 3b). Peak-to-peak amplitude of this long-term response is 8 μrad, whereas the short-term response has amplitudes of <2 μrad. I111 tilt signal seems to be composed of at least two time responses. A short-term time response, similar to that of I144, is detectable by the slope change immediately after rainfall events (see Figure 3b). A medium-term time response is expressed by the pulse responses reaching their maximums 20 days after rainfall events (see Table 2). Finally, a longer-term response similar to that of I144 may exist. This signal cannot be identified clearly because the aforementioned medium-term signal is of larger amplitude.

4. Elastic Parameters Determination

[25] Tilt responses are associated with rainfall events on all instruments. It is likely that much of the deformation signal is associated with the elastic response of the karst system. Elastic properties of the karst medium therefore need to be quantified. To do this, we rely on the principle that a surface load deforms the underlying media and induces measurable tilt at depth. This tilt signal depends on the relative position of the applied load with respect to the instrument and the elastic parameters of the study area.

[26] We conducted a loading experiment at the INFRUTS site to induce measurable tilts. Farming tractors were used as the loading apparatus and were successively stationed on eight loading sites (Figure 4a). Tractors were left at a given site for at least 4 min, which was long enough for the tiltmeters to reach a stable value (Table 3). Sites were loaded with 10, 17.5, or 25 tons, depending on the number of tractors present (Table 3). Tractor masses were taken from the manufacturer's specifications, and the surface area for each tractor was measured. The loading of site HB (Figure 4a) did not produce measurable tilt and is taken as a reference. Measured tilts are corrected for Earth tides.

[27] Residual measured tilt variations have magnitudes of $<5 \times 10^{-8}$ rad. To interpret these tilts, we assume that underground deformation occurs according to the surface loading of a homogeneous elastic half-space. We acknowl-

Table 3. Loading Sites, Mass at Loaded Site, Start and End of Loading, and Chronology for the Tractor Experiment

Site Name	Mass (Tons)	Start	End	Load Chronology
HB	17.5	1036	1044	1
L3	10	1050	1054	2
L3	17.5	1055	1059	3
HB	17.5	1101	1112	4
N1	17.5	1114	1118	5
K4	17.5	1121	1127	6
L4	17.5	1129	1137	7
K2	17.5	1137	1144	8
N2	17.5	1149	1156	9
L2	25	1156	1202	10
N1	25	1204	1212	11
HB	25	1212	1221	12

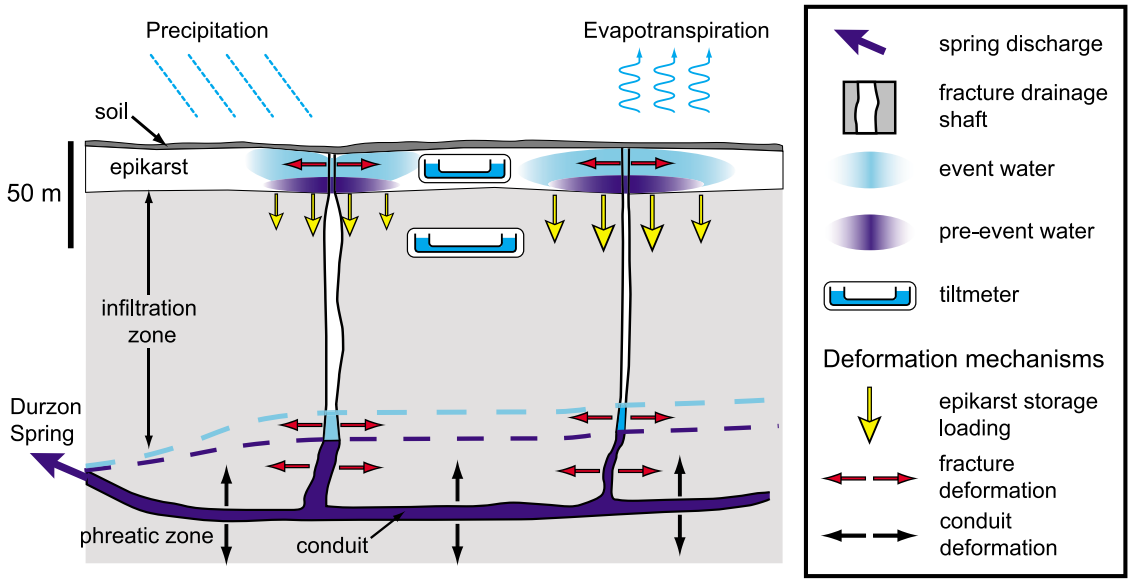

Figure 5. Schematic cross section of the studied karst system showing the different hydrology-related deformation mechanisms. Deformation mechanism arrows represent the strain caused by the addition of event water (light blue), whereas pre-event water (dark blue) represents the state prior to the event rainfall. Not to scale for horizontal distances. (Durzon spring is located at the base of the plateau's rim.)

edge that this model is simplified because of the topography around the site. Also, the presence of a cave in which the tiltmeter is installed is likely to disturb the displacement field locally [*Harrison*, 1976]. In addition, possible spatial variations of elastic constants through the medium may affect tilts.

[28] We refer to the displacement solution in an elastic half-space for a rectangular surface load [*Becker and Bevis*, 2004; *Boussinesq*, 1885]. Tractors are modeled as rectangular surface loads. Within an elastic half-space, a surface loading induces a tilt scaling with $(\lambda + 2\mu)/[\mu(\lambda + \mu)]$ [*Becker and Bevis*, 2004; *Boussinesq*, 1885]. Because loads (tractors) and their position relative to the tiltmeters are precisely controlled, elastic parameters can be obtained by a regression analysis between observed and modeled tilts. To overcome the tradeoff between Lamé parameters λ and μ, we assume a Poisson ratio within a range of 0.2–0.3.

[29] Figure 4b represents observed versus modeled tilt responses for the best fitting parameters for tiltmeter I144. Unfortunately, during the experiment performed in September 2008, the I111 instrument was malfunctioning and is therefore not used in the analysis. Among all sites, the response of the site K4 is opposite to what is predicted by the half-space model for load chronology 6 (see Table 3 and Figure 4b). Considering the vicinity of this site to the chamber in which the tiltmeter is installed, this anomalous tilt response is likely to be due to a cavity effect as discussed by *Harrison* [1976]. To investigate such an effect, we modeled the surface loading at site K4 with a medium including a void using a finite element code ADELI [*Hassani et al.*, 1997], and we indeed observed an inverse tilt response compared to a homogeneous model around the void from this modeling. Furthermore, an anomalous tilt response is observed only when the load is in the direct vicinity of the cavity, and other loading sites do not fall into this case. For these reasons, we choose to exclude the I144 response of site K4 in the regression analysis.

[30] Within the homogeneous half-space hypothesis, elastic parameters that best account for observed tilts on both instruments are $\mu = 2.65 \times 10^9$ and $\lambda = 3.42 \times 10^9$ Pa, corresponding to a Young's modulus of 6.44×10^9 Pa and a Poisson ratio of 0.288. The coefficient of determination R^2 of the regression analysis between I144 measured versus modeled tilt is 0.68 (Figure 4b). In the following section, we use the inverted elastic coefficients as model parameters.

5. Identifying Tilt Mechanism With Finite Element Modeling

[31] The aim of this section is to determine which mechanism may be responsible for the observed tilt signal. We examine the following mechanisms: surface loading and deformation induced by fracture water pressure (Figure 5). Our analysis is done with ADELI code (http://www.dstu.univ-montp2.fr/PERSO/chery/Adeli_web) in its 2-D plane strain version (version 3.4). Special care was taken to validate FEM solutions with analytical solutions [*Becker and Bevis*, 2004], showing RMS differences $<2.5 \times 10^{-8}$ rad. Unfortunately, very little a priori information on epikarst storage properties and fracture location is available around the tilt stations. Tilts from the forthcoming modeling therefore are presented as maximum and averaged amplitudes over large horizontal distances for any given depths.

5.1. Epikarst Loading

[32] Changes of near-surface water mass generate tilt through elastic deformation. At a large scale, ocean tides generate loading that deform the Earth's surface and therefore create tilt [*Llubes et al.*, 2008]. At a smaller scale, tilt deformation has been observed in the Gulf of Corinth and has been associated with waves [*Boudin*, 2004; *Rerolle et al.*, 2006]. At the hydrological catchment scale, tilt signals have been attributed to differential water storage [*Longuevergne*, 2008]. Indeed, gravity loading can generate tilt if a load

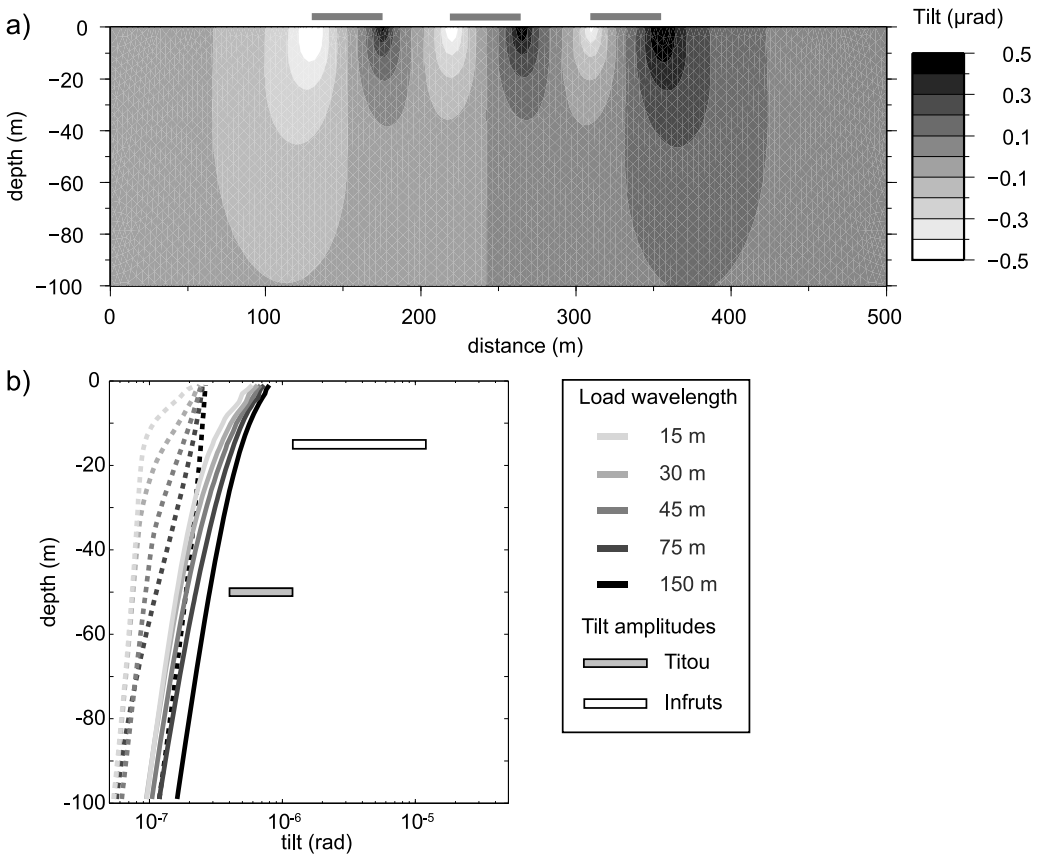

Figure 6. (a) Model cross section showing tilt for a 45 m length scale loading of 0.2 m of water. (b) Modeled tilt versus depth for each loading periodicity, solid lines and dashed lines represent, respectively, maximum and average tilt amplitudes. INFRUTS and TITOU observed tilt amplitude ranges are represented.

gradient exists. Suppose that the epikarst is the main storage entity and that rainfall is uniform. If the storage properties of the epikarst only varied with depth, no horizontal tilt would be generated. Slow and fast draining zones due to the large heterogeneity of all karst systems must therefore be invoked to create a nonuniform loading. This loading effect is represented in Figure 5 by yellow arrows. Differential gravity loading due to spatially variable storage properties leads to tilt deformation and is now investigated.

5.1.1. Model Setup

[33] A rectangular 500 m length by 300 m depth model meshed with some 20,000 triangular elements was constructed. The bottom side of the model is held fixed for both normal and tangential components of motion, whereas lateral sides are only fixed for their normal (i.e., horizontal) motion. Therefore the medium is free to move vertically under loading according to its elastic properties. Because the spatial distribution of the storage properties in the vicinity of each site is unknown, different loading length scales are tested. Different experiments in which the surface of the model space was loaded with repeated loads of lengths 15, 30, 45, 75, and 150 m and separated by the same lengths were done. Applied loads correspond to an equivalent of 200 mm water height (2×10^3 Pa). This load typically represents a heavy precipitation event (see Figure 3) on the karst system. We used elastic parameters inferred from the tractor loading experiment (see section 4). The tilt deformation inside the medium is calculated using the derivative of the vertical motion with respect to the horizontal direction for each element center. Figure 6a represents model tilt for a 45 m periodicity loading scenario up to a depth of a 100 m. Tilt related exclusively to elastic deformation and not to gravity equipotential disturbances is modeled. It has been shown that the deviation of the vertical has an effect about 7 times less important than the elastic deformation effects on tilt for the Preliminary Reference Earth Model (PREM) [*Dziewonski and Anderson*, 1981]) conditions [*Longuevergne*, 2008]. In our case, because elastic parameters are much less than those of PREM, the contribution of equipotential surface tilt is negligible (<2% of the total signal).

5.1.2. Results

[34] Maximum and mean tilt amplitude values, calculated in a central zone 100 m away from the left and right boundaries to avoid boundary effects, are shown for each loading experiment as a function of depth (Figure 6b). Maximum tilts are observed where the load gradients are maximum, that is, in the direct vicinity of the boundary between loaded and unloaded zones (Figure 6a). The larger the loaded surface, the higher the modeled tilt. However, in no case does the modeled tilt, even for its maximum values, reach the observed tilt ranges at the tiltmeter depths (Figure 6b). Measured and modeled tilt comparison clearly suggests that observed tilt amplitudes on both sites cannot be accounted for with epikarst gravity loading mechanism (see Figure 6b).

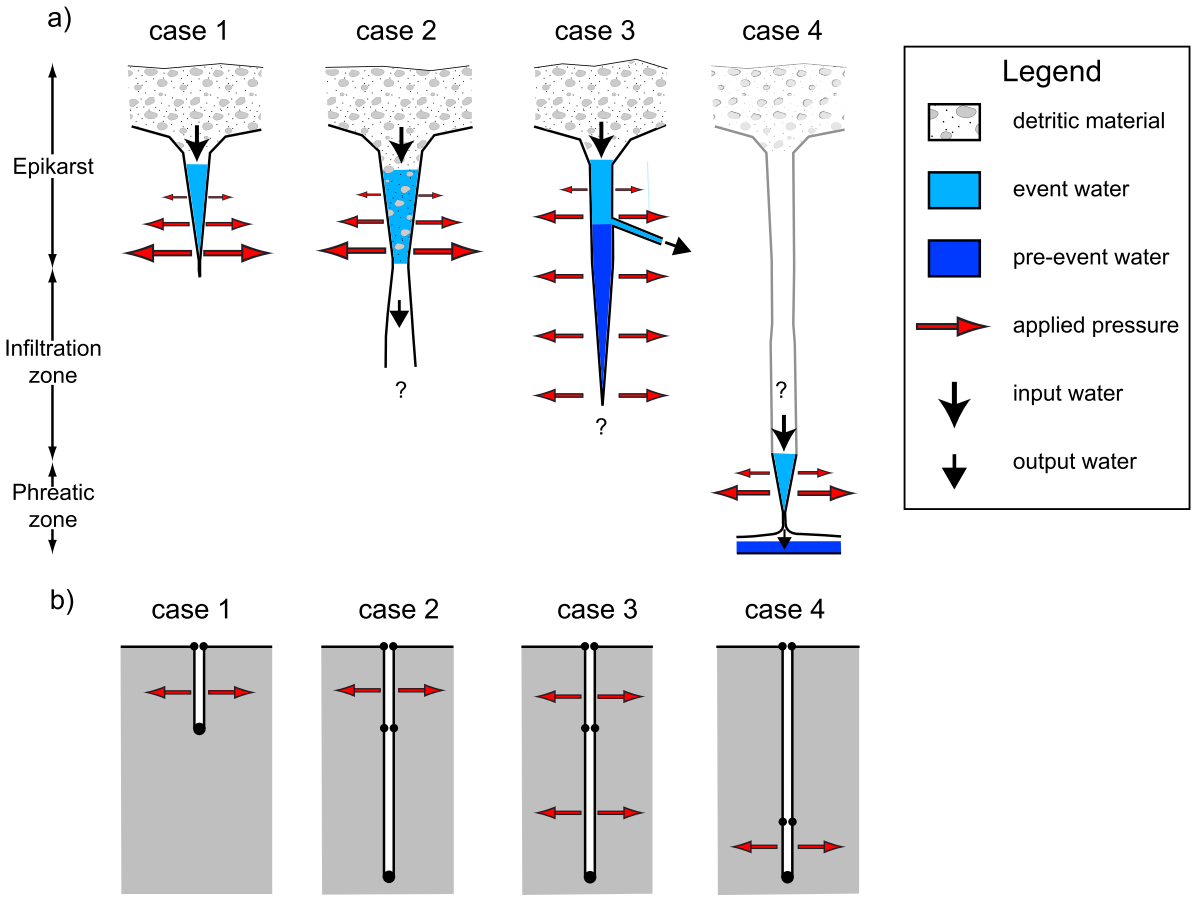

Figure 7. (a) Diagrams of the four fracture cases considered. Vertical distances are not to scale. Red arrows represent variation of applied pressure after event water fills the fractures, pre-event water being already present. (b) Numerical configurations for the four considered cases; nodes are represented as black dots.

[35] As load wavelength decreases, maximum observed tilt amplitude decreases. This is in part due to the fact that combined tilts from two adjacent loading areas compensate, thus resulting in a smaller tilt. A uniform loading, i.e., an infinite loading wavelength, leads to a null tilt in the absence of cavities.

[36] It must be emphasized that this modeling represents extreme conditions that are unlikely to be met on the karst recharge area. Indeed, having zones that are not loaded after rainfall means that these zones do not store any water, which is unrealistic. Our modeling therefore represents the highest loading gradient possible after a 200 mm precipitation event, and therefore the highest possible tilt amplitude. Furthermore, our 2-D modeling represents the effect of infinitely elongated loading structures: A 3-D modeling with finite dimension loads would surely yield lower amplitude tilts. This modeling therefore implies that observed tilts are too large to be the consequence of loading by a saturated patch of epikarst.

5.2. Fracture Deformation

[37] It is well established that water pressure changes in fractures induce bulk deformation of the surrounding rock [*Davis*, 1983; *Evans and Wyatt*, 1984; *Longuevergne et al.*, 2009]. However, a karst embeds various kinds of voids that can be responsible for strain when they are filled by water. A first class of voids corresponds to chambers, conduits, and potholes that are accessible to speleologic exploration. Because of the high degree of connectivity of these conduits, they are generally not filled by water unless they are in the phreatic zone. They are therefore unlikely to produce a strain due to transient water storage in the unsaturated zone. Another common type of voids corresponds to fractures. In this region, these fractures are predominantly of tectonic origin. They may correspond to open fractures within the epikarst, such as those formed from decompression and dissolution [*Williams*, 2008]. On the Larzac plateau, these fractures are ubiquitous and form a vertical network as attested by direct field observation in caves and at the surface. It is generally thought that fractures play an important role in concentrating infiltration from distributed rainfall to channeled infiltration and flow [*Klimchouk*, 2004; *Williams*, 2008]. This is represented as red arrows in Figure 5. Because of the complexity of existing water pathways in a karst system, the key role of pressurized fractures for creating tilt may appear elusive. However, some lines of evidence lead us to conjecture that pressurized fractures are a likely source of strain. First, the variable seasonal water drip of stalactites often corresponds to the outlet of fissures as seen in various caves [*Genty and Deflandre*, 1998]. This suggests at least that these fissures have variable flow rates. Also, we analyze

Table 4. Loaded Fracture Attributes for the Three Modeled Cases[a]

	Fracture Dimensions	Loaded Zone	Applied Load	Fracture Periodicity	Number of Fractures
Case 1	0 to 15 m	0 to 15 m	7.5×10^4 Pa	150, 45, 15	1, 6, 17
Case 2	0 to 150 m	0 to 15 m	7.5×10^4 Pa	None	1
		0 to 15 m	7.5×10^4 Pa	None	1
Case 3	0 to 150 m	15 to 150 m	15×10^4 Pa		
Case 4	0 to 150 m	135 to 150 m	7.5×10^4 Pa	None	1

[a]See section 5.2.1 for explanations.

aerial photographs around the TITOU site to search for a preferential pattern orientation. A clear maximum occurs for directions oriented between N130 and N140 [*Gerbaux*, 2009] that are perpendicular to the tilt orientation recorded after large rain events (see Figure 3c). We therefore consider fracture deformation as a plausible mechanism for the observed tilts and numerically test this hypothesis.

[38] We acknowledge that a variety of pressurized sources may be able to account for a single tilt measurement. As discussed above, these pressurized sources may be karstic voids such as underground chambers, shafts, conduits, or bedding plane partings, but also fractures. The inversion of the source geometry on the basis of tilt data alone is severely underdetermined. However, vertical planar fracture geometries acting as pressure sources are appealing because such fracture geometries are commonly seen underground and on aerial photographs. Also, a thin planar fracture produces a significant tilt in the perpendicular direction with a limited amount of water generating hydrostatic pressure. By contrast, a nonplanar source of pressure, like a point or a line, applies pressure over a limited surface and is a less efficient configuration to deform the surrounding media with the same applied pressure.

5.2.1. Model Setup

[39] Four fracture loading cases are tested (Figure 7):

[40] 1. In case 1, solutionally widened joints that taper downward exist in the epikarst [*Williams*, 2008] and are bound to fill up with water after rainfall events. The fracture is closed, and the fracture faces are clamped together at the base of the epikarst in the model space (fracture tip) (Figure 7b).

[41] 2. In case 2, hydraulically active fractures that convey fast infiltration through the infiltration zone are rooted at the base of the epikarst [*Klimchouk*, 2004; *Williams*, 1985, 2008]. Such fractures may be locally filled with detritic material within the epikarst, so they can fill up with water after heavy rainfall events. Pressure is therefore applied at the top of these open fractures, which are open at the epikarst base.

[42] 3. In case 3, deep penetrating open fractures that taper down at depth but in which water is stored below a given depth are bound to exist. Lateral drains consisting of adjacent fractures or dissolution-widened conduits allow water to exit the system. Water level in such systems therefore varies above the drain and not under it. Hydrostatic water pressure changes arising from water level changes are applied to the whole fracture depth (Figure 7).

[43] 4. In case 4, water level rises occurring at the interface between infiltration and phreatic zones in vertical shafts are also observed in some karst systems and therefore generate pressure variations.

[44] The geometry of the FEM model is identical to the one in section 5.1.1. For case 1, the modeled fracture is vertical and 15 m deep. Fracture depth is set to 15 m because this depth could correspond to a plausible epikarst depth [*Jacob et al.*, 2009; *Williams*, 2008]. Instead of applying a linear hydrostatic pressure on the fracture walls (as is shown in Figure 7a), we apply an average hydrostatic pressure associated with a water column of 15 m, i.e., $\sim 7.5 \times 10^4$ Pa to the fracture walls (see Table 4 and Figure 7b). We test the effects of applying an average and a linearly varying pressure on the fracture wall and find that the deformation field is not significantly modified in the far field, inasmuch as we are examining orders of magnitudes.

[45] We therefore consider that a single rainfall event may cause a 15 m deep vertical fracture to fill up with water completely. As hydrostatic pressure depends only on water height and not on the amount of water, this is plausible. Water level changes of 15 m with a limited amount of water may occur within a thin fracture.

[46] For cases 2 to 4, modeled fractures are 150 m deep (see Table 4), in agreement with the depth of the saturated zone in the northern part of the karst. Pressure corresponding to 15 m of water is applied to the top 15 m of the fracture for cases 2 and 3. The rationale for applying constant pressure rather than linear pressure is explained above.

[47] For case 3, this pressure is also applied from 15 to 150 m depth. This is justified by the fact that the deeper part of the fracture is water filled prior to the rainfall event, and pressure arising from the shallow water level changes is transmitted and applied over the entire below-drain zone (see Figure 7b, case 3). Case 4 consists of fracture loading at depth (see Figure 7b), where a 7.5×10^4 Pa pressure is applied from 135 to 150 m depth at the center of the model.

[48] For case 1, the effect of applying pressure change on the walls of several fractures at repeated length intervals is tested. Fracture loading periodicities of 150, 45, and 15 m corresponding to a total number of, respectively, 1, 6, and 17 fractures are tested. For all other cases, a unique fracture is located at the center of the model. Elastic parameters are those determined by the tractor experiment (see section 4). Lower and lateral boundaries are kept fixed. No initial stress was applied for the model runs, implying that the analysis is focused on differential stress. Indeed, if lithostatic prestress is applied, no tilt response is generated from hydrostatic pressure, because lithostatic confining pressure is much greater (see Table 4), thus preventing the fracture from opening.

5.2.2. Results

[49] Fracture loading modeling yields mean tilt amplitudes that are an order of magnitude higher than those generated from surface loading (compare Figure 6b with Figure 8b). Maximum and mean modeled tilt amplitudes, calculated in the model space 100 m away from the left and

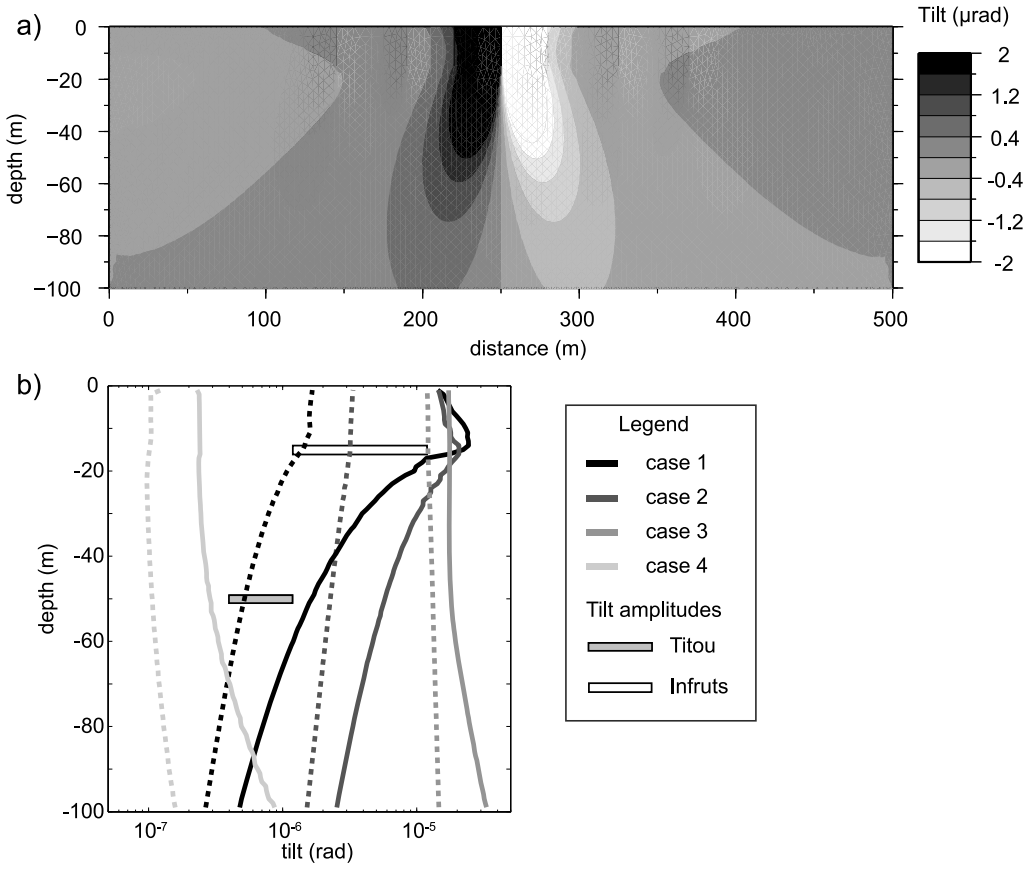

Figure 8. (a) Model cross section showing tilt for a case 1 central fracture loading. (b) Modeled tilt versus depth for each fracture loading case, solid lines are the maximum tilt magnitudes, dashed lines are average tilt magnitudes. INFRUTS and TITOU observed tilt range are represented.

right boundaries to avoid boundary effects, are represented in Figure 8b.

[50] Case 1 scenario yields mean tilts that are comparable to observed tilt amplitudes at the two tiltmeter sites (see Figure 8b). More specifically, mean tilts arising from the loading of 15 m deep fractures are comparable to the observed tilt amplitudes, regardless of the fracture spatial frequency (not shown in Figure 8b). Maximum tilts generated from this case are higher than the observed tilts.

[51] Case 2 scenario yields tilt magnitudes that account well for the INFRUTS site observed tilt, but that are higher than those observed at the TITOU site (see Figure 8b). Indeed, the loading of the upper section of a deep penetrating fracture yields higher tilt deformation than that of a superficial closed fracture under the same loading conditions. For a deep penetrating fracture (case 2 scenario), observed tilts can be accounted for invoking a 9 m water level rise at the uppermost part of the fracture, whereas the filling up of 9 m deep superficial fracture does not account for the observed tilt amplitudes.

[52] Case 3 scenario yields amplitudes that are slightly higher than those observed at INFRUTS sites. Tilt does not decrease with depth over the top 100 m of the model, and so TITOU site amplitudes are much lower than those predicted by the model. This is explained by the fact that pressure is being applied over a great surface for this case (from 0 to –150 m depth), and therefore deformation occurs over a much greater area. Furthermore, maximum and average tilts are calculated over a distance as far as 150 m away from the loaded fractures. Tilt generated from case 3 scenario accounts for the TITOU site tilt amplitude if the fracture is farther than 150 m from the tiltmeter (see section 5.3).

[53] The case 4 scenario yields tilt amplitudes that are smaller than the observed tilts, barely so for the TITOU site and by more than an order of magnitude for INFRUTS site. This scenario may have accounted for TITOU tilt amplitudes if a larger load would have been applied over a greater area at depth, yet INFRUTS site tilt amplitudes cannot be accounted for invoking this case.

[54] Despite the scarcity of our tilt observations, our modeling suggests that shallow fracture loading seems to be a plausible mechanism accounting for the observed tilt amplitudes on both sites. For any given loaded fracture, tilt varies with distance to the fracture (see Figure 8a). We now examine how this constrains the distance between the installed instruments and the loaded fracture for cases 1 to 3.

5.3. Constraints on Pressurized Fracture Location Relative to Tiltmeter Location

[55] The aim of this section is to determine orders of magnitude for the maximum horizontal distance between installed tiltmeters and vertical pressurized fractures that may be responsible for the observed tilt using FEM results.

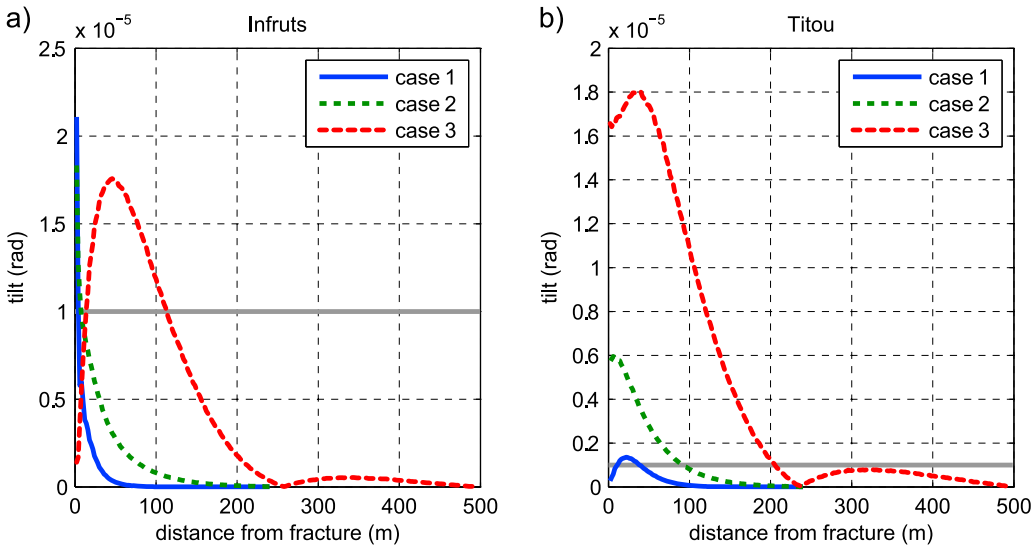

Figure 9. (a) Tilt amplitude as a function of distance from active fracture at INFRUTS depth for the different fracture scenarios. Fractures are loaded with an equivalent of 15 m of water. The horizontal line represents maximum observed tilt variation at INFRUT site. (b) same as Figure 9a for TITOU depth and site.

Cases 1 to 3 are examined, with loading parameters shown in Table 3. Maximum distance is defined as the greatest distance at a given tiltmeter site depth for which modeled tilt equals observed tilt amplitude. Figure 9 represents tilt as a function of distance for different fracture loading scenarios at the INFRUTS and TITOU depths. The maximum distances are the intersections between the observed tilt amplitudes and the tilt versus distance curves for each fracture loading scenario.

[56] For a 15 m loaded case 1 fracture, obtaining INFRUTS site tilt amplitude of 10^{-5} rad means that the tiltmeter must be placed no farther than 4 m away from the fracture (Table 5). For this same scenario, the tiltmeters must be placed at most 11 to 38 m away from the fracture to account for TITOU tilt amplitudes. A range is obtained because the tilt to distance curve has a pulse shape (see Figure 9).

[57] Accounting for the observed tilts with the case 2 scenario implies that the tiltmeters at INFRUTS be no farther than 8 m away from the loaded fracture and 92 m away for TITOU tiltmeters. For the case 3 scenario, tiltmeters at INFRUTS must be placed between 14 and 113 m away from the fracture and no farther than 205 m for TITOU site (Table 5).

[58] It is important to point out that all our calculations have been done for vertical fractures of infinite length. Although field observation suggests that most of the fractures in this part of the Larzac plateau are vertical, they have by no means infinite horizontal extensions. Therefore the distance between the fracture and a tiltmeter that we compute is probably a maximum value. Also, fracture dip influences the strain field as discussed by *Longuevergne et al.* [2009]. The minimum distance also depends on this parameter. Finally, minimum distances vary greatly, depending on the pressure source geometry, its relative position to the instruments, and the magnitude of the applied pressure. Furthermore, we applied a mean constant pressure rather than a depth-dependent pressure; this has an influence on tilt distribution in the near field. For all of the above reasons, the distances given above yield orders of magnitude rather than well-controlled estimates.

[59] A few lessons can be drawn from this modeling:

[60] 1. Deeply rooted open fractures deform the media at longer length scales than shallow fractures with comparable loaded areas.

[61] 2. The larger the area of applied pressure, the larger the deformation length scale. This is clearly illustrated by comparing case 2 and case 3 modeled tilt results (see Figure 9).

[62] 3. The considered fracture scenarios and their full loading by water account for the observed tilt amplitudes if the instruments are at most ~200 m away for the deep site and ~100 m away for the shallow site. If indeed the modeled fracture loading scenarios occur in the field, then installed tiltmeters must be at most 200 m away from these fractures. This exemplifies the local scale sensitivity of these instruments.

[63] In conclusion to this section, fracture loading seems to be a likely mechanism accounting for observed tilt amplitudes. Tilt time response with respect to hydrological parameters is now investigated.

6. Reservoir Lumped Modeling

[64] In this section, the tilt signal is used to determine time constants relative to reservoir discharge properties, which we link to water level changes in hydraulically active fractures. We describe a reservoir lumped model explaining

Table 5. Maximum Distance Between Tiltmeter and Fracture for Different Fracture Scenarios for INFRUTS and TITOU Depths

	Case 1	Case 2	Case 3
INFRUTS	4 m	8 m	14–113 m
TITOU	11–38 m	92 m	205 m

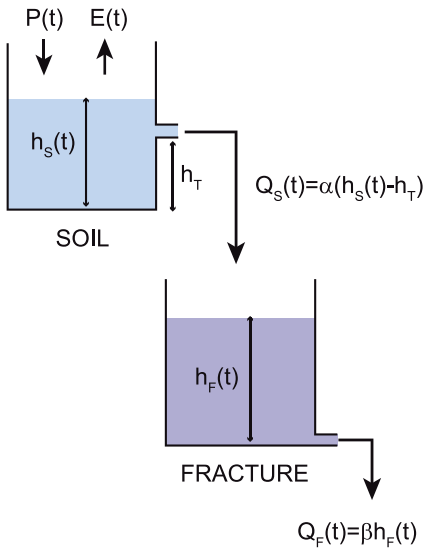

Figure 10. Soil fracture reservoir model (see section 6.2 for explanation).

short- and long-term time constants associated with tilt data.

6.1. Model Rationale

[65] Hydrological lumped models are composed of virtual reservoirs and are aimed at explaining the behavior of a hydrological entity without describing the complex internal physical processes occurring within the system (see, e.g., GR4J [*Perrin*, 2003]; IHACRES [*Jakeman et al.*, 1990]). The aim of such modeling is to determine parameters of the reservoirs that best account for an observed output response. Usually, spring or river discharge, being relatively easy to measure and having integrative properties over a hydrological system, is used as the calibration element. In this study, available input data are rainfall and potential evapotranspiration, but fracture discharge and head are unknown. We assume that tilt signal is related to water level change in neighboring fractures, and we use it as a calibration element for the model. We choose to model fracture water level using a soil reservoir and a fracture reservoir (Figure 10), and we assume that only fracture water level in the model h_F contributes to the tilt. Let S be the drainage area that feeds the fracture, w the fracture width, and L its horizontal length. The relationship between actual water level h and model water level h_F is given by the following equation:

$$h = \frac{S}{wL} h_F, \tag{1}$$

for which water level is therefore linearly related to actual fracture water level.

6.2. Fracture Reservoir Model

[66] To model water level change in a fracture, we built a two-reservoir model comprising a soil and a fracture reservoir (Figure 10) in which the water levels are respectively $h_S(t)$ and $h_F(t)$.

[67] Both soil and fracture reservoir discharges are proportional to water level according to the Maillet model [*Maillet*, 1905] and are expressed as follows:

$$Q_S(t) = \alpha(h_S(t) - h_T), \tag{2}$$

$$Q_F(t) = \beta h_F(t), \tag{3}$$

where α and β are the soil and fracture discharge constants (s^{-1}), and Q_S and Q_F are the discharges (mm s^{-1}) exiting, respectively, the soil and the fracture reservoirs. Transfer from the soil reservoir to the fracture reservoir occurs only if the water level in the soil reservoir is higher than a threshold value h_T. Rainfall P(t) is the model input which is intercepted by the soil reservoir. Part of this water returns to the atmosphere through actual evapotranspiration, and another part feeds the underlying fracture through infiltration. Actual evapotranspiration E(t) is calculated using Penman-Monteith's formula [*Penman*, 1948] for daily potential evapotranspiration scaled by *Turc*'s [1961] yearly total actual evapotranspiration [see *Jacob et al.*, 2008]. Water level in the soil reservoir is given by the following equation:

$$h_S(t) = h_S(t_0) + \int_{t0}^{t} [P(t) - E(t) - Q_S(t)]dt. \tag{4}$$

Water level in the fracture reservoir is defined as follows:

$$h_F(t) = h_F(t_0) + \int_{t0}^{t} [Q_S(t) - Q_F(t)]dt. \tag{5}$$

We iteratively solve equations (2)–(5) using rain data recorded at the BLAQ site (see Figure 1) and potential evapotranspiration provided by Météo-France. Parameters that need to be adjusted are h_T, α, and β and the initial water levels in the soil and fracture reservoirs.

6.3. Tilt Model

[68] Both pressure and fracture wall surface on which pressure is applied vary with water level, the result being an integral relationship linking the fracture water level to tilt. For the sake of simplicity and because our model is largely conceptual, we assume here a linear relation between water level and tilt.

[69] The abundance of open fractures in the karst system makes it likely that more than one fracture generates tilt on the installed instruments as depicted in Figure 11. The resulting tilt associated to strain coming from N fractures may be written as follows:

$$T = \sum_{i=1}^{N} K_i h_{Fi}, \tag{6}$$

where K is a geometric factor combining fracture size, distance, and orientation with respect to the tiltmeter. Because no a priori choice can be made for N, we adopt a heuristic attitude consisting of searching for the minimum complexity model that yields a unique optimal solution in the parameter

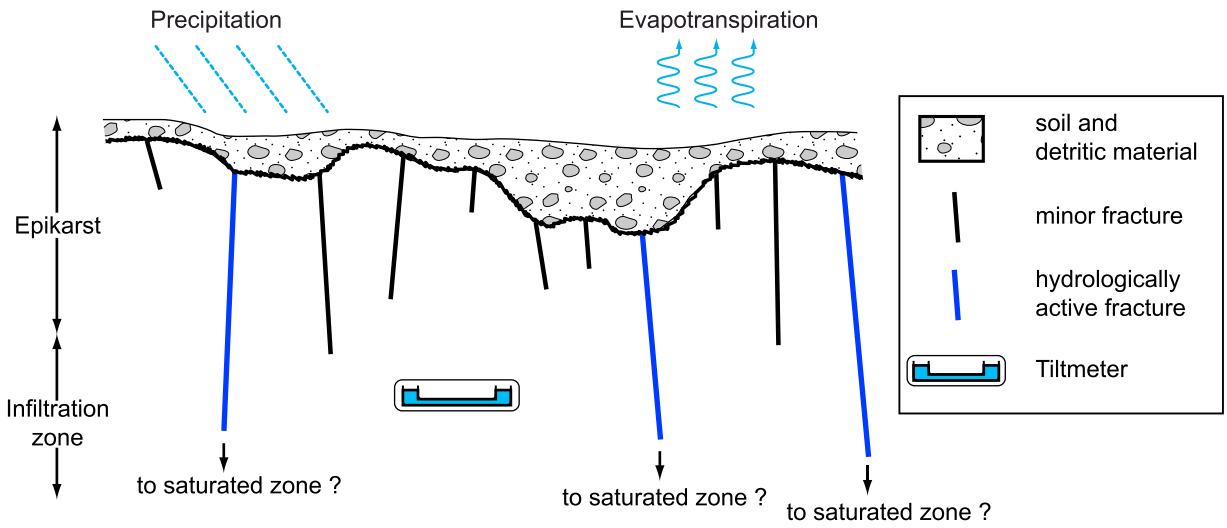

Figure 11. Schematic of karst upper zone showing hydraulically active fractures.

space. An optimal model solution accounts for observed tilt signals with a minimum number of fractures.

[70] We find that observed tilts cannot be accounted for using a single fracture model ($N = 1$), and that a two-fracture lumped model ($N = 2$) incorporates enough degrees of freedom to account for the observed signal. Equation (4) can be reformulated as follows:

$$T = K_1 h_{F1} + K_2 h_{F2}, \tag{7}$$

where h_{F1} and h_{F2} are the water levels in the fractures models and K_1 and K_2 are two unknown constants. Six parameters therefore need to be inverted: threshold soil values h_{T1} and h_{T2}, soil discharge constants α_1 and α_2, and fracture discharge constants β_1 and β_2. In addition, four initial values for the soil and fracture reservoir need to be inverted. We perform a Monte Carlo sampling on these parameters using the Mersenne Twister pseudorandom number generator [*Matsumoto and Nishimura*, 1998], and run the two lumped models yielding fracture water levels h_{F1} and h_{F2}. Finally, we least square adjust K1 and K2, and the modeled tilt is compared to the observed tilt. The best set of parameters is the one that minimizes the normalized root mean square error between observed and modeled tilt.

6.4. Results: INFRUTS

[71] Results of the best fit inversions are shown in Table 6. For the I144 tilt signal, best fitting short-term and long-term models are governed by soil discharge constants of, respectively, 1.1 and 143.9 days and fracture discharge constants of, respectively, 6.6 and 147.2 days (Table 6). Soil threshold values are, respectively, 149 mm and 152 mm. Figure 12a shows the best fit model and its decomposition for the two fractures for I144 tiltmeter. The inversion yields decomposition into short- and a long-term components that are clearly visible in the observed tilt as discussed in section 3.3.

[72] For I111 tilt data, best fitting models are governed by soil discharge constants of, respectively, 11.7 and 108.5 days and fracture discharge constants of, respectively, 189.6 and 190.8 days. Soil threshold values are, respectively, 158 mm and 237 mm. Figure 12b shows the best fit model and its two components for I111 tiltmeter.

[73] It is interesting to note that constant K_2 is negative for this tiltmeter. The opposite signs of K_1 and K_2 denote that the tilt-generating fractures are likely located on opposite sides of the instrument. As a result, the decomposition of the tilt signal is not intuitively inferred by looking at the tilt response of I111.

6.5. Results: TITOU

[74] Results for T094 tiltmeter are shown in Table 6. The modeling did not yield acceptable results for the T012 tiltmeter; we chose therefore not to include it. This is due to the strong decrease after November 2006 (Figure 3a). This may either be an instrumental drift or our model does not represent all the hydrological processes at TITOU.

[75] The inversion reveals best fit parameters of 0.9 and 1.4 days for soil discharge, 5.3 and 52 days for fracture discharge, and soil threshold values of 110.1 and 322 mm (Table 6) for the two modeled fractures, respectively. The modeled tilt with its two fracture components is plotted on Figure 13.

7. Discussion

[76] Good temporal correlation between precipitation events and tilts on TITOU and INFRUTS underground sites strongly suggests that tilt signals are hydraulically induced.

Table 6. Inverted Model Parameters for INFRUTS and TITOU Tiltmeters for the Different Power Law Exponents

Instrument	α_1^{-1} (d)	β_1^{-1} (d)	h_{T1} (mm)	α_2^{-1} (d)	β_2^{-1} (d)	h_{T2} (mm)	Normalized RMS (%)	K_1	K_2
I144	1.1	6.6	149	143.9	147.2	152	4.45	$2.75\ 10^{-2}$	$6.20\ 10^{-2}$
I111	11.7	189.6	158	108.5	190.8	237	3.44	$8.34\ 10^{-2}$	$-6.74\ 10^{-2}$
T094	0.9	5.3	110.1	1.4	52.0	322.0	4.83	$1.56\ 10^{-3}$	$2.80\ 10^{-3}$

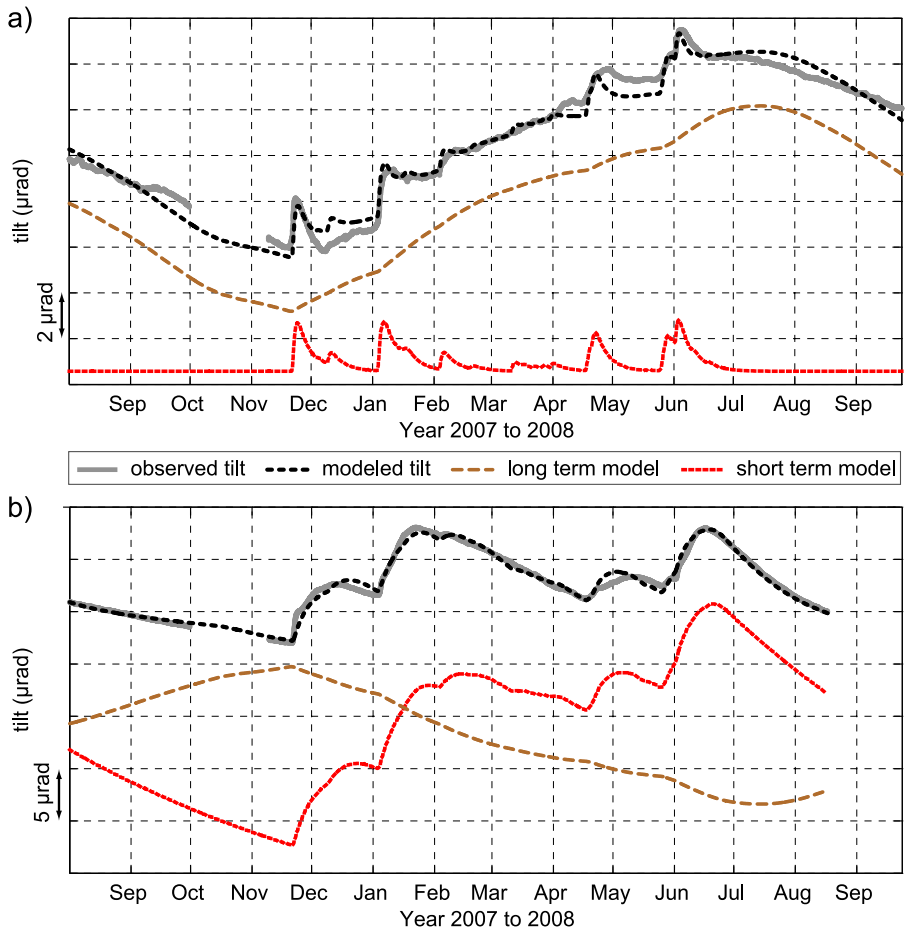

Figure 12. Best fit model (black dashed line) and its two fracture components (brown and red dashed lines) confronted to observed tilt (solid gray line) for (a) I144 tiltmeter and (b) I111 tiltmeter. Fracture signals are shifted vertically for better legibility.

Direct loading due to near-surface water storage cannot generate observed tilt amplitudes. Pressurized voids within the karst must be invoked to explain the signal. Emphasis must be placed on the fact that the pressurized source geometry cannot be determined from tiltmeter data alone. Because of the ubiquity of vertical fractures in the karst system, our preferred interpretation is that the hydromechanical response of fractures is responsible for the observed tilt signal. Using a theoretical soil-fracture model for fracture filling and emptying, we determine effective time constants associated with their behavior. In the following text, we attempt to link our interpretation to the heterogeneity and fracture density of the vadose zone. We then discuss the possible link between the local hydraulic behavior and the global karst discharge dynamics.

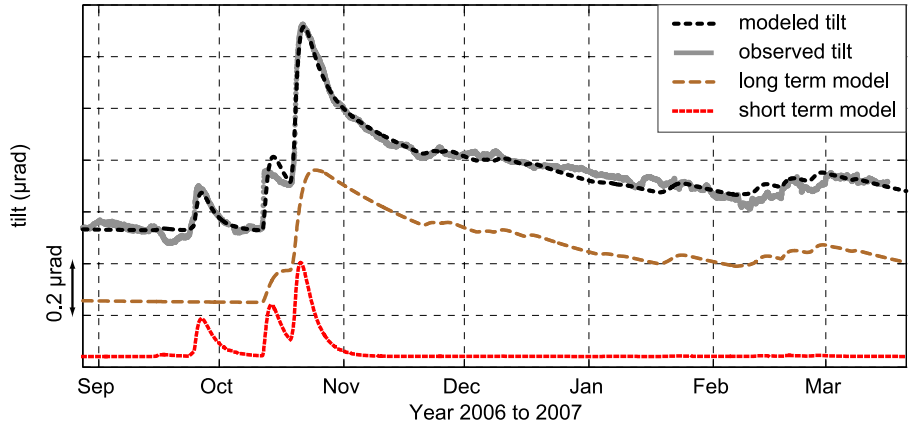

Figure 13. Best fit model and its two fracture components confronted to observed tilt for T094 tiltmeter.

[77] Tiltmeters are sensitive to global strain such as earth tides as well as local strain induced by hydraulic perturbations. At a local scale, the tilt response created by a pressure source within an elastic half-space decreases with respect to the source distance. Using in situ values of elastic parameters for the vadose zone, 2-D plane strain modeling led us to suggest that vertical fractures, if they are responsible for the observed tilt, are likely to be within 100–200 m of the instruments. Observed tilts may therefore be the signature of local water transfer processes in the vadose zone. Suppose there are several hydraulically conductive fractures in the tiltmeter vicinity. Only the closest and more active ones should dominate the composite signal seen by the instruments. The limit case of this interpretation is provided by *Longuevergne et al.* [2009], who invoked a single fracture to explain the tilt observed in a mine.

[78] Another important aspect of the tilt response is that shallow instruments (here 15 m depth for the INFRUTS site) display a much larger tilt amplitude (~10 μrad) than deeper ones (we measure ~1 μrad at 50 m depth). This observation may be interpreted by invoking shallow active fractures as the sole tilt-generating features in the karst system. This conjecture is supported by two independent arguments. First, numerous observations in karst areas reveal that perched aquifers are trapped in the epikarst [*Klimchouk*, 2004; *Williams*, 2008] and may correspond to the hydraulic scheme of Figure 7 (cases 1 and 2). Another element has recently been provided by surface and underground gravity measurements in the vicinity of the present study sites [*Jacob et al.*, 2009]. These measurements suggest that most of the time dependent gravity signal is generated by water storage at shallow depth (the top 60 m) rather than a deeper storage in the vadose or phreatic zone. Therefore our preferred interpretation is that tiltmeters installed in the TITOU site at some 50 m depth lay at larger distances from the pressure sources (plausibly active fractures) than do tiltmeters installed at INFRUTS site, hence accounting for amplitude differences between the two sites.

[79] Although we interpret the observed tilts at depth with respect to the internal structure of the vadose zone, it must be emphasized that strain and tilt amplitude decrease with depth is a general feature of subsurface crustal strain [*Johnson et al.*, 1995]. Indeed, strain is generally high in nonsaturated areas, precisely because the time-dependent saturation chiefly causes strain variation.

[80] After precipitation events, the rapid tilt response of T094 and I144 may indicate that rapid hydrological processes are occurring, such as fractures filling rapidly. One major question is whether fracture orientation can be inferred from tilt measurements. Because the azimuth of the maximum tilt remains constant during short-term responses (Figures 3c and 3d), water level change in a single fracture may be responsible for the observed tilt. Nonetheless, the question of the orientation of active fractures cannot be solved as a variety of dips and orientations may explain the tilt data [*Longuevergne et al.*, 2009]. We observe that most dissolution-enlarged fractures in the considered areas are nearly vertical. Considering the active fractures to be vertical, the azimuth of the tilt vector in its vicinity should be perpendicular to the fracture orientation. This could indicate a N130° to N140° fracture direction for both TITOU and INFRUTS site on the basis of the N40° to N50° tilt azimuth (Figures 3c and 3d). To our knowledge, fractures with this direction are not reported on the Larzac plateau [*Constantin et al.*, 2002]. However, unpublished work conducted by our group on preferential directions associated with surface fractures inferred from aerial photographs in the Durzon basin shows that N10° and N130° directions are dominant [*Gerbaux*, 2009]. Further geophysical investigations in the vicinity of tiltmeter stations should bring new insight into the relationship between hydraulically active karst fractures and associated strain.

[81] Characteristic time constants of karst springs are usually determined from hydrograph analysis. Because spring flow integrates the behavior of the recharge area as a whole, the derived time constants are thought to be representative of the average behavior of the karst system. Tiltmeters, owing to their sensitivity to local pressure sources, may help characterize local water transfer. Within the fracture hypothesis, the determination of input and output fluxes from these fractures may be determined. Whereas a karst spring hydrograph is the integration of all processes occurring on the karst, tiltmeters are representative of local karst functioning.

[82] INFRUTS tilt signal can be decomposed as the sum of at least two time-varying signals which have different time scales, possibly related to the functioning of nearby infiltration pathways and processes. This site illustrates the heterogeneous state of shallow karst hydrological processes, where fast infiltration pathways (time scales <10 days) and slow infiltration pathways (time scales of >100 days) coexist. This quantifies the proposition of *Klimchouk* [2004], who claims that epikarst plays a major role in separating and distributing flow as fast and slow infiltration. Furthermore, a preferential water storage zone may exist in the surroundings of the INFRUTS site in the temporary lakes area (see Figure 1). This area may contribute to the recession part of the Durzon hydrograph [*Jacob et al.*, 2008]. The long-term response at INFRUTS site could hence be related to this slow infiltration.

[83] For the TITOU site, the short-term events (1 day) are most likely the signature of fast infiltration waters feeding fractures. TITOU short-term tilt response and Durzon spring flood are not in phase (Figure 3a), because the spring flood represents transfer through open conduits that correspond to the fastest flow through the system. Spring flood events represent the integral of all fast infiltration and withdrawal, whereas tiltmeters' short-term response may be one of these fast infiltration pathways.

[84] Future studies would benefit from the use of several colocalized instruments: tiltmeters, strainmeters, extensometers, and underground hydrological instrumentation such as flowmeters. Furthermore, the record of longer tilt time series is mandatory to obtain a good understanding of seasonal and annual karst behavior. Ideally, if a set of tiltmeters were installed every kilometer on the Durzon karst, the understanding of the functioning of this karst would be greatly enhanced. However, long-base tiltmeters depend on preexisting caves for their installation. One way to overcome this limitation would be to use borehole tiltmeters. With such instruments, the karst recharge area would not only be much more densely covered, but tilt signal could also be recorded at different depths within a borehole. With this technique, preferential pathways of infiltrating waters and active fractures could be studied much more precisely. However,

these instruments do not yet have the time stability to monitor long term (>1 month) hydraulically induced tilt.

8. Conclusions

[85] Tiltmeters installed in karst media bring original information on karst functioning. We find that a direct water load on the subsurface is unlikely to account for observed tilt amplitudes. Rather, tilt signal may be caused by pressure variations in nearby water pathways such as fractures, hence providing novel information on local karst functioning. Using simple lumped modeling, we have successfully accounted for the observed tilt signals. Several components of local infiltration water may be inferred from the tilt data: fast infiltration, which plausibly feeds the spring high flow events, and slow infiltration, which is part of the base flow component of the spring discharge. Major hydraulically active pressurized sources can therefore be detected, yet their positioning is not possible with one set of tiltmeters alone.

[86] **Acknowledgments.** This manuscript was greatly enhanced by the comments of anonymous reviewers. This project was part of the program Ecosphère Continentale funded by the Agence Nationale de la Recherche. The town council of La Couvertoirade (Aveyron, France) is warmly thanked for its support of the project. We are indebted to J.-L. Rocher for his advice on numerous cave locations, G. Barrau for his invaluable help in installing the tiltmeters, and P. Vernant for his help in the field. The tractor experiment would not have been possible without R. Calazel. We also express our gratitude to L. Longuevergne and N. Florsch for many fruitful conversations.

References

Agnew, D. (1986), Strainmeters and tiltmeters, *Rev. Geophys.*, *24*, 579–624.

Bakalowicz, M. (2005), Karst groundwater: A challenge for new resources, *Hydrogeol. J.*, *13*(1), 148–160.

Becker, J., and M. Bevis (2004), Love's problem, *Geophys. J. Int.*, *156*, 171–176.

Boudin, F. (2004), Développement et validation d'un inclinomètre longue base de subsurface à silice et mercure: Application à des mesures géophysiques de haute résolution sur le chantier pilote du Golfe de Corinthe., Ph.D. dissertation, 322 pp., Inst. de Phys. du Globe de Paris, Paris.

Boudin, F., P. Bernard, L. Longuevergne, N. Florsch, C. Larmat, C. Courteille, P. A. Blum, T. Vincent, and M. Kammentaler (2008), A silica long base tiltmeter with high stability and resolution, *Rev. Sci. Instrum.*, *79*(3), 11.

Boussinesq, J. (1885), *Application des Potentiels à l'Étude de l'Équilibre et du Mouvement des Solides Élastiques*, Gauthier-Villars, Paris.

Braitenberg, C. (1999), Estimating the hydrologic induced signal in geodetic measurements with predictive filtering methods, *Geophys. Res. Lett.*, *26*(6), 775–778, doi:10.1029/1999GL900064.

Braitenberg, C., G. Romeo, Q. Taccetti, and I. Nagya (2006), The very-broad-band long-base tiltmeters of Grotta Gigante (Trieste, Italy): Secular term tilting and the great Sumatra-Andaman islands earthquake of December 26, 2004, *J. Geodyn.*, *41*, 164–174.

Bruxelles, L. (2001a), Reconstitution morphologique du Causse du Larzac (Larzac central, Aveyron, France): Rôle des formations superficielles dans la morphogenèse karstique, *Karstologia*, *38*, 25–40.

Bruxelles, L. (2001b), Dépôts et altérites des plateaux du Larzac central: Causses de l'Hospitalet et de Campestre (Aveyron, Gard, Hérault): Evolution morphogénique, conséquences géologiques et implications pour l'aménagement, Ph.D. dissertation, 266 pp., Univ. de Provence, Aix-en-Provence, France.

Constantin, J., P. Vergély, and J. Cabréra (2002), Tectonique et fracturation associée dans le bassin des Causses (Aveyron, France): Le cas du secteur de Tournemire, *Bull. Soc. Géol. France*, *173*(3), 229–243.

Dal Moro, G., and M. Zadro (1998), Subsurface deformations induced by rainfall and atmospheric pressure: Tilt/strain measurements in the NE-Italy seismic area, *Earth Planet. Sci. Lett.*, *164*, 193–203.

Davis, P. (1983), Surface deformation associated with a dipping hydrofracture, *J. Geophys. Res.*, *88*(B7), 5829–5834, doi:10.1029/JB088iB07p05826.

Denic-Jukic, V., and D. Jukic (2003), Composite transfer functions for karst aquifers, *J. Hydrol.*, *274*(1–4), 80–94.

D'Oreye, N. F., and W. Zurn (2005), Very high resolution long-baseline water-tube tiltmeter to record small signals from Earth free oscillations up to secular tilts, *Rev. Sci. Instrum.*, *76*(2), 12.

Dziewonski, A., and D. Anderson (1981), Preliminary Reference Earth Model (PREM), *Eos Trans. AGU*, *62*(17), 332.

Evans, K., and F. Wyatt (1984), Water table effects on the measurement of Earth strain, *Tectonophysics*, *108*, 323–337.

Fabian, M., and H.-J. Kümpel (2003), Poroelasticity: Observations of anomalous near surface tilt induced by ground water pumping, *J. Hydrol.*, *281*(3), 187–205, doi:110.1016/S0022-1694(1003)00234-00238

Fleury, P., M. Bakalowicz, and M. Becker (2007a), Characterising a karst system with a submarine spring: The example of La Mortola (Italy), *Comptes Rendus Acad, Sci. Geosci.*, *339*(6), 407–417.

Fleury, P., V. Plagnes, and M. Bakalowicz (2007b), Modelling of the functioning of karst aquifers with a reservoir model: Application to Fontaine de Vaucluse (South of France), *J. Hydrol.*, *345*(1–2), 38–49.

Genty, D., and G. Deflandre (1998), Drip flow variations under a stalactite of the Pere Noel cave (Belgium): Evidence of seasonal variations and air pressure constraints, *J. Hydrol.*, *211*(1–4), 208–232.

Gerbaux, G. (2009), Impact de la fracturation et de la karstification sur la dynamique des eaux souterraines dans le Larzac, Master's thesis, 39 pp., Univ. Montpellier II, Montpellier, France.

Harrison, J. C. (1976), Cavity and topographic effects in tilt and strain measurement, *J. Geophys. Res.*, *81*(2), 319–328, doi:10.1029/JB081i002p00319.

Hassani, R., D. Jongmans, and J. Chéry (1997), Study of plate deformation and stress in subduction processes using two-dimensional numerical models, *J. Geophys. Res.*, *102*(B8), 17,951–17,965, doi:10.1029/97JB01354.

Jacob, T., R. Bayer, J. Chéry, H. Jourde, N. Le Moigne, J. P. Boy, J. Hinderer, B. Luck, and P. Brunet (2008), Absolute gravity monitoring of water storage variation in a karst aquifer on the Larzac plateau (Southern France), *J. Hydrol.*, *359*(1–2), 105–117, doi:110.1016/j.jhydrol.2008.1006.1020.

Jacob, T., J. Chéry, R. Bayer, N. Le Moigne, J. P. Boy, P. Vernant, and F. Boudin (2009), Time-lapse surface to depth gravity measurements on a karst system reveal the dominant role of the epikarst as a water storage entity, *Geophys. J. Int.*, *177*, 347–360.

Jakeman, A. J., I. G. Littlewood, and P. G. Whitehead (1990), Computation of the instantaneous unit-hydrograph and identifiable component flows with application to 2 small upland catchments, *J. Hydrol.*, *117*(1–4), 275–300.

Jeannin, P. Y. (2001), Modeling flow in phreatic and epiphreatic karst conduits in the Holloch cave (Muotatal, Switzerland), *Water Resour. Res.*, *37*(2), 191–200, doi:10.1029/2000WR900257.

Johnson, H., F. Wyatt, D. C. Agnew, and W. Zurn (1995), Tidal tilts at Piñon Flat, California measured at depths of 24 and 120 meters, paper presented at 12th International Symposium on Earth Tides, Science Press, Beijing.

Jukic, D., and V. Denic-Jukic (2006), Nonlinear kernel functions for karst aquifers, *J. Hydrol.*, *328*(1–2), 360–374.

Klimchouk, A. (2004), Towards defining, delimiting and classifying epikarst: Its origin, processes and variants of geomorphic evolution, Proceedings of the Symposium held October 1–4, 2003 Sheperdstown, West Virginia, USA, *Karst Water Inst. Spec. Publ., Epikarst*, *9*(1), 23–25.

Labat, D., R. Ababou, and A. Mangin (2000a), Rainfall-runoff relations for karstic springs: part II. Continuous wavelet and discrete orthogonal multiresolution, *J. Hydrol.*, *238*(3–4), 149–178.

Labat, D., R. Ababou, and A. Mangin (2000b), Rainfall-runoff relations for karstic springs: part I. Convolution and spectral analyses, *J. Hydrol.*, *238*(3–4), 123–148.

Legchenko, A., J. M. Baltassat, A. Beauce, and J. Bernard (2002), Nuclear magnetic resonance as a geophysical tool for hydrogeologists, *J. Appl. Geophys.*, *50*, 21–46.

Llubes, M., et al. (2008), Multi-technique monitoring of ocean tide loading in northern France, *C. R. Geosci.*, *340*(6), 379–389.

Longuevergne, L. (2008), Contribution a l'hydrogéodésie, Ph.D. dissertation, 300 pp., Univ. Pierre et Marie Curie, Paris.

Longuevergne, L., N. Florsch, F. Boudin, L. Oudin, and C. Camerlynck (2009), Tilt and strain deformation induced by hydrologically active natural fractures: Application to the tiltmeters installed in Sainte-Croix-aux-Mines observatory (France), *Geophys. J. Int.*, *178*(2), 667–677.

Maillet, E. (1905), *Essais d'Hydraulique Souterraine et Fluviale*, 218 pp., Hermann, Paris.

Mangin, A. (1975), Contribution à l'étude hydrodynamique des aquifères karstiques, Ph.D. dissertation, 124 pp., Univ. de Dijon, Dijon, France.

Matsumoto, M., and T. Nishimura (1998), Mersenne twister: A 623-dimensionally equidistributed uniform pseudorandom number generator, *ACM Trans. Model. Comput. Sim.*, *9*(1), 3–30.

Michelson, A. A. (1914), Preliminary results of measurements of the rigidity of the earth, *Astrophys. J.*, *39*, 105–138.

Penman, H. L. (1948), Natural evaporation from open water, bare soil and grass, *Proc. R. Soc. London*, *193*, 120–145.

Perrin, J. (2003), A conceptual model of flow and transport in a karst aquifer based on spatial and temporal variations of natural tracers, Ph.D. dissertation, 227 pp., Univ. of Neuchâtel, Neuchâtel, Switzerland.

Plagnes, V. (1997), Structure et fonctionnement des aquifères karstiques. Caractérisation par la chimie des eaux., Ph.D. dissertation, 372 pp., Univ. of Montpellier II, Document du BRGM no. 294, Montpellier, France.

Rerolle, T., N. Florsch, M. Llubes, F. Boudin, and L. Longuevergne (2006), L'inclinométrie, un nouvel outil pour le suivi temporel des aquifères?, *Comptes Rendus Acad. Sci. Geosci.*, *338*, 775–786.

Ricard, J., and M. Bakalowicz (1996), Connaissance, aménagement et protection des ressources en eau du Larzac septentrional, Aveyron (France), 94 pp., BRGM, Orléans, France.

Turc, L. (1961), Evaluation des besoins en eau d'irrigation, évapotranspiration potentielle, *Ann. Agronom.*, *12*(1), 13–49.

Van Camp, M., P. Meus, Y. Quinif, O. Kaufman, M. Van Ruymbeke, M. Vandiepenbeeck, and T. Camelbeek (2006), Karst aquifer investigation using absolute gravity, *Eos Trans. AGU*, *87*(30), 298.

Weise, A., G. Jentzsch, A. Kiviniemi, and J. Kaariainen (1999), Comparison of long-period tilt measurements: results from the two clinometric stations Metsahovi and Lohja, Finland, *J. Geodyn.*, *27*(2), 237–257.

Wenzel, H.-G. (1996), The Nanogal software: Earth tide data processing package ETERNA 3.30., *Bull. d'Inf. Marées Terr.*, *124*, 9425–9439.

Westerhaus, M., and W. Welle (2002), Environmental effects on tilt measurements at Merapi volcano, *Bull. d'Inf. Marées Terr.*, *137*, 10917–10926.

Williams, P. W. (1983), The role of the subcutaneous zone in karst hydrology, *J. Hydrol.*, *61*, 45–67.

Williams, P. W. (1985), Subcutaneous hydrology and the development of doline and cockpit karst, *Z. Geomorphol.*, *29*, 463–482.

Williams, P. W. (2008), The role of the epikarst in karst and cave hydrogeology: A review, *Int. J. Speleol.*, *37*(1), 1–10.

Yamauchi, T. (1987), Anomalous strain response to rainfall in relation to earthquake occurrence in the Tokai area, Japan, *J. Phys. Earth*, *35*(1), 19–36.

Zadro, M., and C. Braitenberg (1999), Measurements and interpretations of tilt-strain gauges in seismically active areas, *Earth Sci. Rev.*, *47*, 151–187.

R. Bayer, F. Boudin, and J. Chéry, Géosciences Montpellier, UMR CNRS/UM2 5243, Université Montpellier II, Montpellier, France.

T. Jacob, Department of Physics and Cooperative Institute for Research in Environmental Sciences, University of Colorado, PO Box 216, Boulder, CO 80309-0216, USA. (thomas.jacob@colorado.edu)